Chemical Science

ROYAL SOCIETY OF CHEMISTRY

EDGE ARTICLE

View Article Online
View Journal | View Issue

Cite this: *Chem. Sci.*, 2024, **15**, 13191

All publication charges for this article have been paid for by the Royal Society of Chemistry

Accurate construction of monolayer, bilayer, sandwich bilayer, four-layer, multi-layer and chiral bilayer 2D pillararene-type supramolecular networks†

Zhao-Nian Chen,‡[a] Le-Ping Zhang,‡[a] Huai-Li Wu,[a] Qiao-Yan Qi,[b] Meng Yan,[c] Jia Tian,[b] Guan-Yu Yang,[a] Zhan-Ting Li *[bd] and Bo Yang *[a]

The accurate construction of mono-, bi- and multi-layer networks has been an important challenge, especially for bi- and multi-layer networks. Monolayer, bilayer, sandwich bilayer, four-layer, and multi-layer two-dimensional pillararene-type metal–organic coordination networks have been constructed from functionalized pillar[5]arene and pillar[6]arene by utilizing the coordination interaction of cobalt and copper ions and combining with temperature control and guest induction. These two-dimensional coordination networks exhibit the excellent plasticity of pillararenes and structural variety, which are characterized by X-ray single crystal diffraction and PXRD, confirming that pillararenes units can function as excellent tunable scaffolds for structural regulation. Two-dimensional chiral double-layer structure products are also constructed from *R*- and *S*-pillar[6]arene, which are obtained by high-performance liquid chromatography. Atomic force microscopic imaging confirms the thicknesses of these networks. Moreover, these networks also exhibit high iodine adsorption capacity in aqueous environments at ambient temperature. The monolayer, bilayer, sandwich bilayer, four-layer and multi-layer structures of the pillararene-type networks represent a new facile supramolecular self-assembly strategy and platform for designing more mono-, bi- and multi-layer two-dimensional nanomaterials and chiral two-dimensional double-layer structures provide a new method for the construction of more two-dimensional chiral polymers.

Received 8th May 2024
Accepted 4th July 2024

DOI: 10.1039/d4sc03022b

rsc.li/chemical-science

Introduction

Since the emergence of graphene monolayer materials,[1] research towards developing more types of monolayer two-dimensional (2D) materials has exploded.[2,3] These 2D materials usually exhibit exceptional performance in diverse applications due to their distinct structural characteristics of ultrathin thicknesses, enormously high surface areas, and well-defined 2D extended skeletons. Controlling the arrangement, thickness, or number of monolayers also played a crucially important role, especially when the designed function involves electron or energy transfer between the adjacent monolayers,[4,5] so direct access to mono-, bi- and multi-layer structures remains an important challenge in constructing 2D materials. At the same time, it is more challenging to use one compound to accurately control monolayers and bilayers, or construct adjustable double-layer, four-layer and multi-layer structures by adjusting their structure, especially for bilayer, four-layer and multilayer structures. Supramolecular host macrocycles are a special class of ring structures,[6–9] which can be modified on the ring to adjust the size of the cavity according to the size of the guest molecule, have been used in constructing bilayer sheets.[10–12] Kian Ping Loh and co-workers introduced a viologen threading unit based on crown ethers and reported that the formation of a host–guest complex facilitates the self-exfoliation of covalent organic frameworks (COFs) into crystalline monolayers or bilayers.[10] Zhao *et al.* constructed a unique Janus bilayer 2D supramolecular organic framework through self-assembly of amphiphilic tritopic molecules and cucurbit[8]uril.[11] We also realized the hierarchical self-assembly of a bilayer 2D supramolecular organic framework in

[a]*College of Chemistry, Zhengzhou University, 100 Kexue Street, Zhengzhou, Henan, 450001, China. E-mail: yangbohy@zzu.edu.cn*

[b]*Key Laboratory of Synthetic and Self-Assembly Chemistry for Organic Functional Molecules, Shanghai Institute of Organic Chemistry, Shanghai, 200032, China*

[c]*School of Chemistry and Chemical Engineering, Henan University of Technology, Zhengzhou, Henan, 450001, China*

[d]*Department of Chemistry, Shanghai Key Laboratory of Molecular Catalysis and Innovative Materials, Fudan University, 2205 Songhu Road, Shanghai, 200438, China. E-mail: ztli@fudan.edu.cn*

† Electronic supplementary information (ESI) available. CCDC 2244320–2244328, 2326165–2326167, 2326170–2326172, 2326174, 2326175, and 2342430. For ESI and crystallographic data in CIF or other electronic format see DOI: https://doi.org/10.1039/d4sc03022b

‡ Z. N. Chen and L. P. Zhang contributed equally to this work.

a controllable manner through cucurbit[8]uril-encapsulation-promoted dimerization of 4-phenylpyridinium subunits and the coordination of rod-like bipyridine ligands with zinc porphyrin subunits.[12]

Pillararenes, a relatively new class of macrocycles, have shown great promise in host–guest molecular recognition and the fabrication of various materials for divergent applications, since Ogoshi and co-workers reported the first pillararene in 2008.[13–23] The rims of pillararenes are highly customizable, enabling them to be fitted with different substituents for different functions, which significantly facilitates their hybridization into metal–organic networks or pillars.[24–30] Meanwhile the existing several metal–organic networks or pillars are A1/A2-difunctionalized or five para-substituted pillar[5]arenes and the rigid pillar architectures of pillararenes are all maintained. To the best of our knowledge, bi- and multi-layer 2D polymeric architectures by using the cavity of pillararenes as tunable scaffolds by deforming or adjusting the rigid pillar cavity have not been accessed to date. Herein, considering the versatile potential of modification on the rims of pillararenes and the tunability of cavities of pillararenes, we have incorporated pillar[5]arene and pillar[6]arene units as excellent tunable scaffolds into the construction of monolayer, bilayer, and multi-layer coordination networks. In this system, we report the controlled self-assembly of 2D monolayer and 2D bilayer supramolecular coordination networks from a tetrapyridine functionalized pillar[5]arene with Co(II) through controlling the temperature, and the accurate construction of 2D bilayer, 2D sandwich bilayer, 2D four-layer and 2D multi-layer supramolecular coordination polymers from a tetrapyridine functionalized pillar[6]arene with Cu(II) by temperature control and guest induction, and precise chirality control of a 2D *R*-bilayer and a 2D *S*-bilayer supramolecular coordination network by high-performance liquid chromatography.

Results and discussion

The published literature showed that A1/A2-difunctionalized pillar[5]arene is an excellent assembly motif for constructing metal–organic hybrid materials.[24–30] We also found that the dipyridine-functioned pillar[5]arene ligand **P5PhPy2** (ref. 27), which exhibits a compact packing manner in the solid state, could be coordinated with transition metals Cu(II) and Co(II) to afford 1D single-line (**P5PhPy2Cu-1** and **P5PhPy2Cu-2**) at room temperature and parallel double-line (**P5PhPy2Cu-3**) and ladder-like double-line coordination polymeric arrays (**P5PhPy2Cu-4** and **P5PhPy2Co-1**) at 80 °C with good crystallinity under enclosed conditions (Fig. S1–S4†). To extend 1D coordination polymeric arrays to various 2D structures, a symmetrical tetrapyridine functionalized pillar[5]arene ligand (**P5PhPy4**) and pillar[6]arene ligand (**P6PhPy4**) were designed and prepared (Fig. 1), to investigate their coordination with Co(II) and Cu(II), respectively, to afford 2D monolayer, bilayer and multi-layer pillararene-type metal–organic coordination networks (PMOCNs). For the preparation of **P5PhPy4** (Scheme S1†), **2** (ref. 31) was first reduced with $NaBH_4$ and then reacted with triflic anhydride to produce **3** and then further coupled

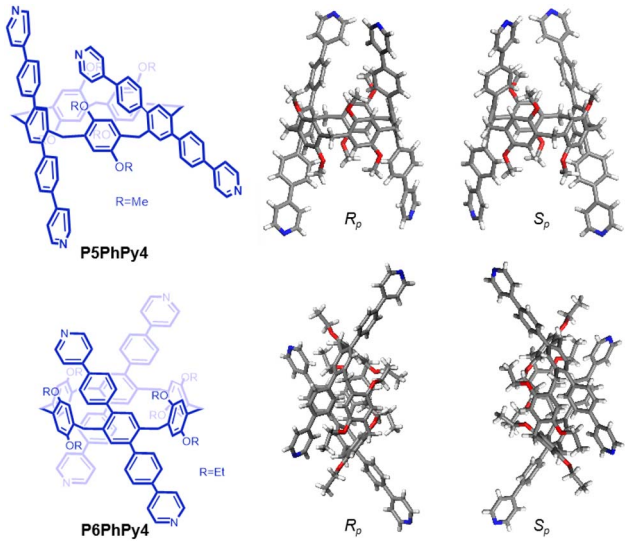

Fig. 1 Compounds **P5PhPy4** and **P6PhPy4** and the crystal structure of **P5PhPy4** (R_p, S_p) and **P6PhPy4** (R_p, S_p).

with 4-(4-pyridyl)phenylboric acid to give rise to **P5PhPy4** in 48% yield. The compound **P6PhPy4** was prepared through coupling of **4** (ref. 32) and 4-(4-pyridyl)phenylboric acid in 40% yield (Scheme S2†).

Crystals of free **P5PhPy4** were obtained as enantiomers (R_p, S_p) *via* slow evaporation from the solution of dichloromethane (Fig. 1) and the cavity of **P5PhPy4** was a perfect well-maintained pentagonal macrocycle. The molecular arrangements of **P5PhPy4** from the top view demonstrated a compact packing manner in the (1,0,0), (0,1,0), and (0,0,1) directions (Fig. S5†). Meanwhile, the pillar[5]arene units of **P5PhPy4** could be used as height adjustable stands to allow for the formation of mono- and bilayer networks (**ml-2D-P5MOCNs** and **bl-2D-P5MOCNs**) under the coordination of Co(II).

The coordination of **P5PhPy4** with Co(II) nitrate in DMF in the presence of acetic acid at 80 °C afforded crystalline products, a monolayer compact coordination network (**ml-2D-P5MOCNs**) (Fig. S6†). X-ray diffraction analysis revealed that the rigid cavity of **P5PhPy4** collapsed to some extent due to the coordination interaction between cobalt and pyridine. The structure of **P5PhPy4** in the crystal of **ml-2D-P5MOCNs** was different from that in the crystal of free **P5PhPy4**; the configuration of two 1,4-dimethoxybenzene units was reversed under coordination at 80 °C, while they were still enantiomers. The two straight ligands of **P5PhPy4** adopted a misaligned parallel orientation, and the torsional angle of the two straight ligands of free **P5PhPy4** changed from 43.26° to close to 0° under coordination interaction (Fig. 2a). There were two types of monolayer structures with three coordinated forms of cobalt in the single crystal of **ml-2D-P5MOCN**: six-coordinate, five-coordinate, and four-coordinate. One type of monolayer network showed Co(II) atoms take six-coordinate and five-coordinate, Co(II) atoms linked two **P5PhPy4** ligands through Co–N bonds (2.102–2.165 Å) to form a –Co–**P5PhPy4**–Co–**P5PhPy4**– rail and such parallel rails were cross-linked by Co–O contacts (1.894–2.222 Å) as "rungs", O atoms from CH_3COO^-

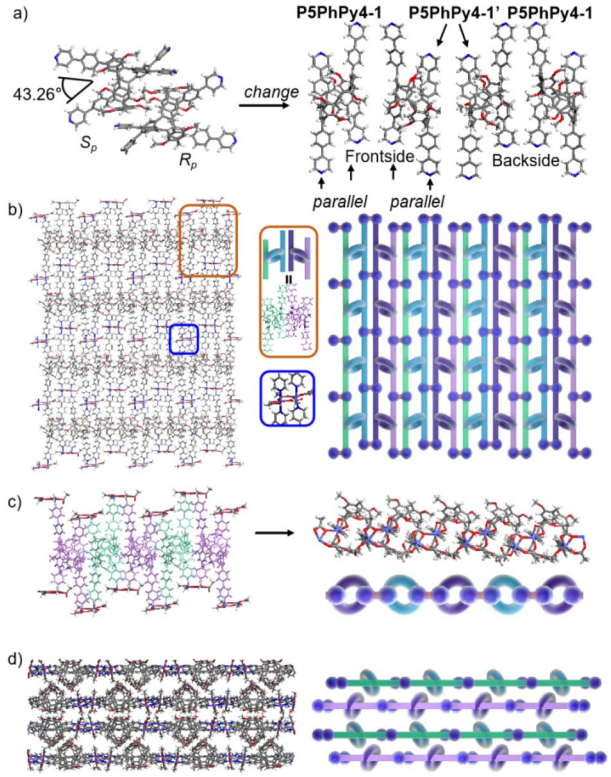

Fig. 2 (a) The transformation of **P5PhPy4** (R_p, S_p) in **ml-2D-P5MOCN**. (b) The top view of a single layer 2D coordination of the polymer **ml-2D-P5MOCN**. (c) The side view of the alternate $-R_p-S_p-R_p-S_p-$ arrangement of the polymer **ml-2D-P5MOCN**. (d) The stacking structure of **ml-2D-P5MOCN**. Noncoordinated solvent molecules are omitted.

(Fig. 2b). The other type of monolayer network showed Co(II) atoms take five-coordinate and four-coordinate form (Fig. S7†), Co(II) atoms linked two **P5PhPy4** ligands through Co–N bonds (2.076–2.199 Å), one type Co–O contacts (1.914–2.312 Å) as "rungs", O atoms from CH_3COO^- and $HCOO^-$, another type Co–O contacts (1.692–2.331 Å) independent, O atoms from CH_3COO^- and H_2O. To be exact, it was the four parallel line group formed by four parallel pillararenes and Co(II), which then formed a 2D structure through hydrogen bonds (Fig. S7b–d†). All these results revealed that two types of independent 2D monolayer structures with Co–N bonds as longitudinal linkers along with a collapsed macrocycle, and Co–O bonds or Co–O bonds and hydrogen bonds (2.105–2.306 Å) as transverse linkers, and the pillar[5]arene units exhibited an alternate $-R_p-S_p-R_p-S_p-$ arrangement (Fig. 2b and c and S7a–c†). Longitudinal side views indicated that the monolayer structures were stacked in the form of dislocation and back to back, due to the outer-surface action of the pillar[5]arene (Fig. 2d). The lateral side view showed that the pillar[5]arene units in the laminated structure were arranged in a micro-helix-like S-shaped curve (Fig. S8†). This result confirmed that pillar[5]arene units could be used as excellent tunable scaffolds to accurately control the monolayer by adjusting the rigid pillar cavity.

As excellent tunable scaffolds, the deformation of the cavity of pillar[5]arene may vary, so we cultured **P5PhPy4** and cobalt nitrate under the same conditions at room temperature. The reaction of **P5PhPy4** with Co(II) nitrate in DMF in the presence of acetic acid at room temperature afforded another different crystalline product, a double-layer metal–organic network **bl-2D-P5MOCN** (Fig. S9†). The X-ray single-crystal structure of **bl-2D-P5MOCN** revealed that this rigid cavity of **P5PhPy4** was greatly deformed due to the coordination interaction between cobalt and pyridine. The torsional angle of the two straight ligands of **P5PhPy4** was changed from 43.26° to 100.78° (Fig. 3a). Due to the existence of the deformed cavity, the two straight ligands of **P5PhPy4** showed a form of parallel up and down crossing, and then a bilayer structure was formed under the coordination of Co(II) (Fig. 3b and S10†). In the bilayer 2D network of **bl-2D-P5MOCN**, the top view presented a quadrilateral grid structure with two layers in the (1,1,0) direction, the upper and lower square-grid windows presented a parallel dislocation form, and the dimensions of the upper and lower square-grid windows were all 24.35 × 24.01 Å. Each of these square-grid windows was constructed from one side ligands of two enantiomers (R_p, S_p) (Fig. 3a). The Co(II) atom was six-coordinate, bonded by four pyridine N atoms from four different **P5PhPy4** ligands (Co–N, 2.156–2.163 Å), one oxygen donor from H_2O (Co–O, 2.096 Å), and another oxygen donor from nitrate ions (Co–O, 2.153 Å) (Fig. 3b). H_2O and NO_3^- were located above and below the cobalt, and the upper layer was

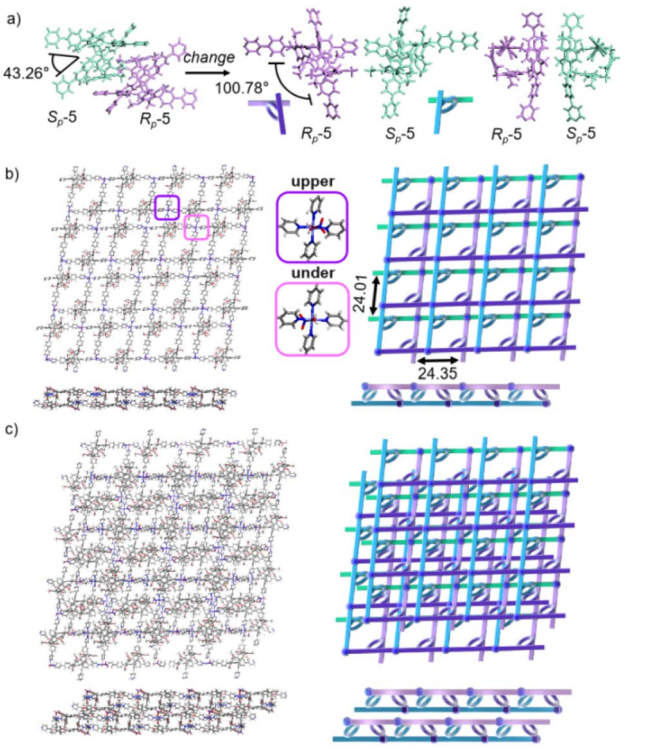

Fig. 3 (a) The transformation of **P5PhPy4** (R_p, S_p) in **bl-2D-P5MOCN**. (b) The crystal structure and diagram of a bilayer 2D coordination of the polymer **bl-2D-P5MOCN**. (c) The stacking structure of a bilayer 2D coordination of the polymer **bl-2D-P5MOCN**. Noncoordinated solvent molecules are omitted.

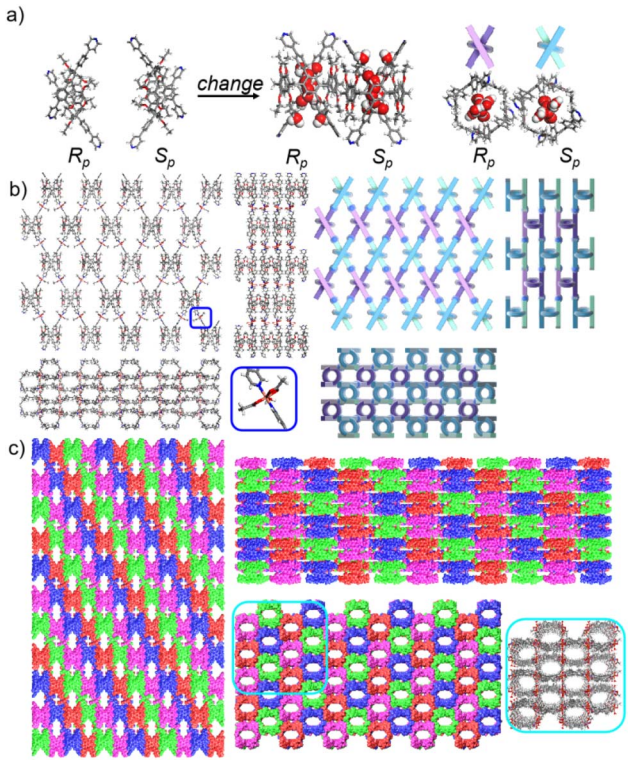

Fig. 4 (a) The crystal structure and diagram of **P6PhPy4** (R_p, S_p) in **mtl-2D-P6MOCN**. (b) The crystal structure and diagram of a multi-layer 2D coordination of the polymer **mtl-2D-P6MOCN**. (c) The stacking structure of a multi-layer 2D coordination of the polymer **mtl-2D-P6MOCN**. Noncoordinated solvent molecules were omitted.

NO_3^- (up) and H_2O (down), while the lower layer was H_2O (up) and NO_3^- (down). The side views presented a clear double-layer form in the (0,0,1) direction. This bilayer structure was an independent 2D bilayer structure with deformed macrocycles as scaffolds. It is worth noting that 2D bilayer networks stacked in a pile-up of dislocations manner (Fig. 3c), presenting a staggered overlapping arrangement of bilayers. The bilayer network further confirmed that pillararene units were excellent tunable scaffolds and could form 2D monolayer and bilayer supramolecular coordination polymers by controlling the temperature.

Crystals of free **P6PhPy4** were obtained as enantiomers (R_p, S_p) *via* slow evaporation from the solution of dichloromethane/methanol (2 : 1), while **P6PhPy4** showed a twisted hexagonal structure (Fig. 1), and the molecular arrangements of **P6PhPy4** were similar to those of **P5PhPy4**, from the top view demonstrating a compact packing manner in the (1,0,0), (0,1,0), and (0,0,1) directions (Fig. S11†). Following the single crystal culture method, **P5PhPy2** with Cu(II) or Co(II), **P5PhPy4** with Co(II), and **P6PhPy4** with Cu(II) nitrate in DMF in the presence of acetic acid at 80 °C for 24 h afforded the crystalline product **mtl-2D-P6MOCN** (Fig. 4a and S12†). The crystal structure of **mtl-2D-P6MOCN** revealed that the cavity of **P6PhPy4** was changed from a twisted hexagonal structure to a perfect well-maintained hexagonal macrocycle under the coordination interaction between copper and pyridine and the modulation of disordered water molecules (Fig. 4a). Due to the perfect well-maintained hexagonal cavity, the two straight ligands of **P6PhPy4** showed a form of parallel up and down crossing, and **P6PhPy4** (R_p, S_p) showed a regular up and down arrangement under coordination interaction, and then a multi-layer structure with staggered and parallel connections of pillararenes was formed (Fig. 4b and S12†). The top view of the structure presented a regular diamond structure in the (1,0,0) direction and each of these diamond windows was constructed from one side ligands of two enantiomers (R_p, S_p) (Fig. 4b). The Cu(II) atom was six-coordinate, bonded by two pyridine N atoms from two different **P6PhPy4** ligands (Co–N, 2.020–2.023 Å), three oxygen donors from CH_3COO^- ions, and one oxygen donor from H_2O (Co–O, 1.788–2.336 Å) (Fig. 4b). The side view showed a parallel multi-layer with a parallel staggered arrangement of **P6PhPy4** in the (0,1,0) and (0,0,1) directions (Fig. 4b). Although this multi-layer structure was formed with perfect well-maintained hexagonal macrocycles as scaffolds, the multi-layer structure stacked in a four-fold interpenetrating form, and the stacking of pillararenes presented multiple metal–organic pillar arrangement forms (Fig. 4c and S13†). The reasonable explanation of the occurrence of such structural interpenetration of **mtl-2D-P6MOCN** was driven by the minimization of the systematic energy through the optimal filling of the void space,[33] which reflected the law that nature abhors a vacuum.

We redissolved the **mtl-2D-P6MOCN** crystals and recultured them under the same conditions at 80 °C for 72 h, affording a new bilayer structure product **bl-2D-P6MOCN**. X-ray diffraction analysis revealed that the pillar[6]arene units of **P6PhPy4** in **bl-2D-P6MOCN** showed a twisted hexagonal structure similar to that of free **P6PhPy4** in the solid state. The two straight ligands of **P6PhPy4** showed a form of parallel up and down crossing similar to **bl-2D-P5MOCN**, and the torsional angle of the two straight ligands approached 120° (Fig. 5a), and then a bilayer structure was formed under the coordination of Cu(II) (Fig. 5b and S14†). The Cu(II) atoms linked **P6PhPy4** ligands through Cu–N (2.162–2.171 Å), Cu–O (1.958–1.992 Å), and Cu–Cu bonds (2.640 Å) to form a –**P6PhPy4**–Cu–Cu–**P6PhPy4**– rail, with O atoms from acetate. Each Cu(II) atom was six-coordinate, with Cu(II) bound to one nitrogen donor from one **P6PhPy4** ligand and four CH_3COO^- ions in a monodentate manner. The Cu–Cu contact completed the six-coordinate Cu center. It is worth noting that this bilayer structure featured an ordered cross arrangement of two sets of parallel lines and the metal coordination was the junction between the ligands, whereas pillar[6]arene played an important role in isolation and linkage. Although **bl-2D-P6MOCN** was also an independent 2D bilayer structure with a deformed macrocycle as scaffolds similar to **bl-2D-P5MOCN**, each independent 2D bilayer network was constructed by single chiral pillararenes (*R*- or *S*-) (Fig. 5c), one 2D bilayer network was constructed by ***R*-P6PhPy4** and another 2D bilayer network was formed through ***S*-P6PhPy4**, presented an antiparallel dislocation stacking arrangement of ***R*-bl-2D-P6MOCN** and ***S*-bl-2D-P6MOCN**. This behaviour may provide more ideas for the construction of 2D single chirality bilayer planar structures (2D-*R* and 2D-*S*) by chiral separation.

To further investigate the possible effect of reaction time, we cultured **P6PhPy4** and copper nitrate under the same conditions

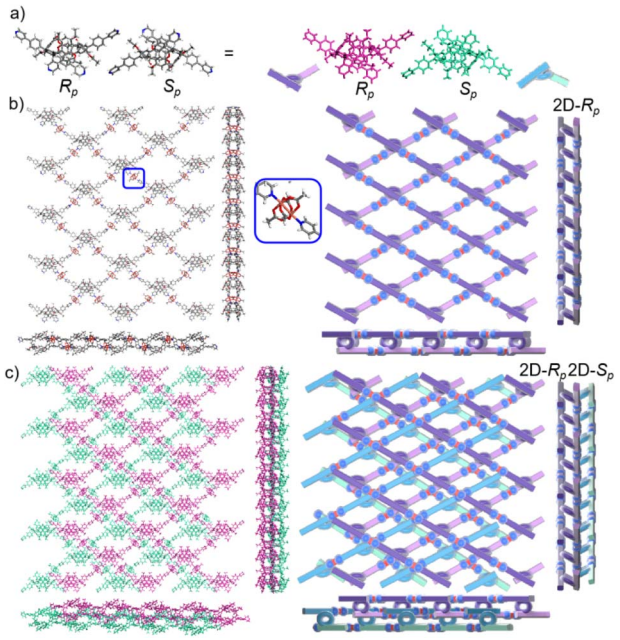

Fig. 5 (a) The crystal structure and diagram of **P6PhPy4** (R_p, S_p) in **bl-2D-P6MOCN**. (b) The crystal structure and diagram of a bilayer 2D coordination of the polymer **bl-2D-P6MOCN** (2D-R_p). (c) The stacking structure of a bilayer 2D coordination of the polymer **bl-2D-P6MOCN**. Noncoordinated solvent molecules were omitted.

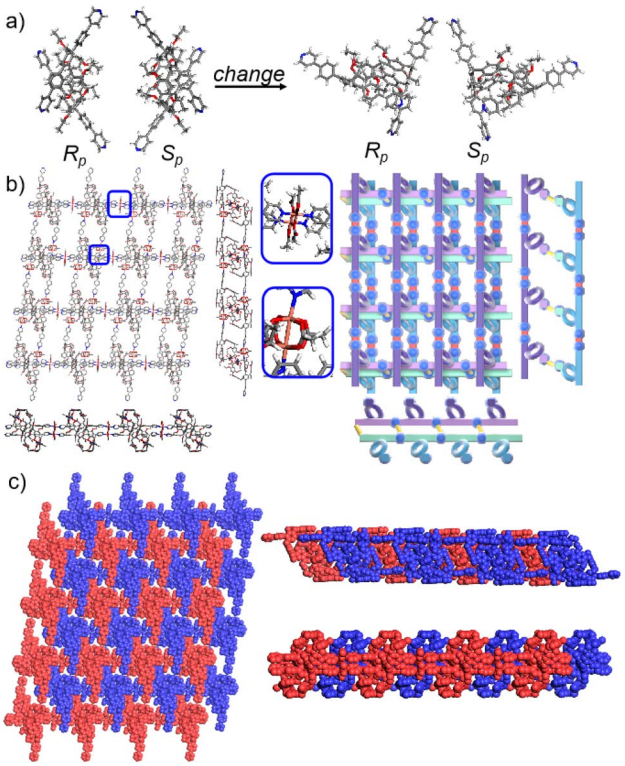

Fig. 6 (a) The crystal structure and diagram of **P6PhPy4** (R_p, S_p) in **fl-2D-P6MOCN**. (b) The crystal structure and diagram of a four-layer 2D coordination of the polymer **fl-2D-P6MOCN**. (c) The four-layer braided two-dimensional network of **fl-2D-P6MOCN** with the up and down entanglement pattern and interlocking pattern. Noncoordinated solvent molecules were omitted.

at 80 °C for 10 days, which afforded a new four-layer structure product **fl-2D-P6MOCN**. The crystal structure revealed that pillar[6]arene units in **fl-2D-P6MOCN** also showed a twisted hexagonal structure in the solid state, while the torsional angle of the two straight ligands of **P6PhPy4** appeared nearly 90° (Fig. 6a and S15†). We have drawn a slightly exaggerated schematic for ease of presentation (Fig. 6b). The two straight ligands of each **P6PhPy4** in **fl-2D-P6MOCN** showed a form of parallel up and down crossing similar to **bl-2D-P5MOCN**, and two **P6PhPy4** molecules, one ***R*-P6PhPy4** and the other ***S*-P6PhPy4**, were arranged in an antiparallel order under the coordination of Cu(II), and then a four-layer structure was formed. There were two link models of Cu(II) in this crystal structure; one link model of Cu(II) atoms and **P6PhPy4** was the same as that of **bl-2D-P6MOCN**, in which Cu(II) atoms linked **P6PhPy4** ligands through Cu–N (2.170–2.183 Å), Cu–O (1.776–1.916 Å), and Cu–Cu (2.654 Å) bonds to form a –**P6PhPy4**–Cu–Cu–**P6PhPy4**– rail, with O atoms from acetate, and there were two such parallel rails at the top and the bottom of the four-layer structure. The other link model of Cu(II) atoms and **P6PhPy4** was a ladder-like model in the middle of the four-layer network, in which the Cu(II) atoms linked **P6PhPy4** ligands through Cu–N bonds (2.010–2.019 Å) to form a –Cu–**P6PhPy4**–Cu–**P6PhPy4**– rail and two such parallel rails of different **P6PhPy4** were cross-linked by Cu–O contacts as "rungs" (1.989–2.328 Å), with O atoms from the acetate ion (Fig. 6b). The Cu(II) atom of the –Cu–**P6PhPy4**–Cu–**P6PhPy4**– rail was also six-coordinate, with Cu(II) bound to two nitrogen donors from two **P6PhPy4** ligands, and the Cu–O contact (1.965–2.711 Å) of Cu(II) and four oxygen donors of three CH_3COO^- ions completed the six-coordinate Cu center. It is worth noting that two four-layer structures formed a more dense four-layer braided two-dimensional structure through interpenetration (Fig. 6c), and the four-layer braided two-dimensional network was stacked in the form of dislocation stacking arrangement layer by layer (Fig. S16†). The molecular woven network adopted the overlying weaving mode with the up-and-down entanglement pattern and innovative interlocking pattern at the same time due to the presence of **P6PhPy4**,[34] which was extremely significant for enriching the weaving types and entanglement patterns of molecular woven structures. Similar to **mtl-2D-P6MOCN**, the structures of **fl-2D-P6MOCN** could also transform into **bl-2D-P6MOCN** through redissolving the crystals of **fl-2D-P6MOCN** and reculturing them under the same conditions at 80 °C for 7 days, while **bl-2D-P6MOCN** could not be returned to **fl-2D-P6MOCN** and **mtl-2D-P6MOCN** and maintained the same structure, meaning that **bl-2D-P6MOCN** may be a more stable form, which may be attributed to the structure of **P6PhPy4** in **bl-2D-P6MOCN** being closest to the free **P6PhPy4** without solvent molecules, representing its lowest energy state.

The pillar[6]arene units of **P6PhPy4** in **bl-2D-P6MOCN** and **fl-2D-P6MOCN** all exhibited twisted hexagonal structures and to transform them into a perfect well-maintained hexagonal macrocycle, we modulated the coordination network by

adopting guest induction.[35] We cultured **P6PhPy4**, adiponitrile and copper nitrate under the same conditions at 80 °C for 3–10 days and then afforded an amazing sandwich bilayer structure product **sbl-2D-P6MOCN** (Fig. 7a and S17†). Unlike **fl-2D-P6MOCN** and **mtl-2D-P6MOCN** effected by reaction time, from 3 days to 10 days, it is still a sandwich bilayer structure, except that the molecules DMF or disordered adiponitrile in the cavity of pillar[6]arene units had changed (Fig. 7 and S18†). X-ray diffraction analysis revealed that the two straight ligands of **P6PhPy4** showed a form of parallel up and down crossing and the coordination pattern of Cu(II) in **sbl-2D-P6MOCN** was similar to that of **mtl-2D-P6MOCN**, a –Cu–**P6PhPy4**–Cu–**P6PhPy4**– model, where the Cu(II) atom was six-coordinate or five-coordinate, bonded by two pyridine N atoms from two different **P6PhPy4** ligands (Cu–N, 1.973–2.066 Å) and four or three oxygen donors from CH_3COO^- ions or CH_3COO^-, COO^- and H_2O (Cu–O, 2.045–2.660 Å). While the arrangement of **P6PhPy4** in **sbl-2D-P6MOCN** was different from that of **mtl-2D-P6MOCN**, **P6PhPy4** showed a coplanar parallel arrangement under coordination interaction, and then an unusual sandwich bilayer structure was formed. Similar to **bl-2D-P6MOCN**, each independent 2D sandwich bilayer structure was constructed from single chiral pillararenes; one was constructed from ***R*-P6PhPy4** and the other was formed from ***S*-P6PhPy4**, and this coordination network also presented an alternating dislocation stacking arrangement of ***R*-sbl-2D-P6MOCN** and ***S*-sbl-2D-P6MOCN** (Fig. 7c, S17 and S18†). The behaviors of **sbl-2D-P6MOCN** and **bl-2D-P6MOCN** not only represented the adjustability of pillar[6]arene, but also further confirmed the feasibility of forming 2D single chirality bilayer planar polymer structures (2D-*R* and 2D-*S*).

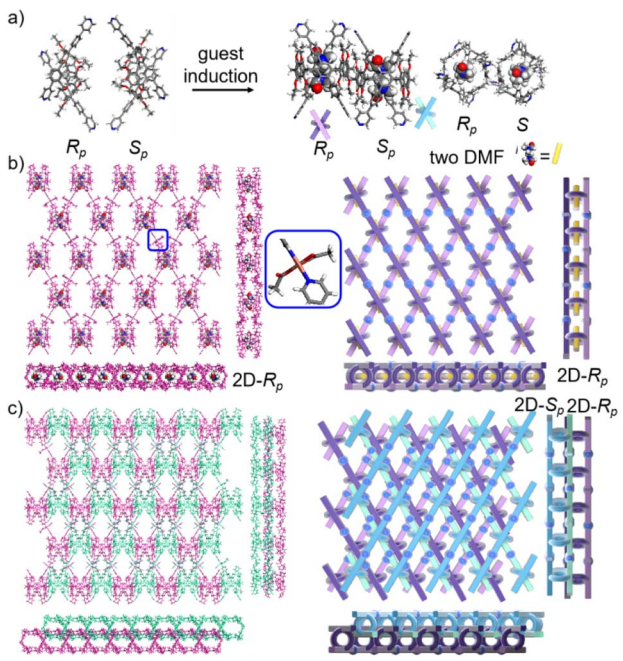

Fig. 7 (a) The transformation of P6PhPy4 (R_p, S_p) in sbl-2D-P6MOCN. (b) The crystal structure and diagram of a sandwich bilayer 2D coordination of the polymer sbl-2D-P6MOCN (2D-R_p). (c) The stacking diagram of a sandwich bilayer 2D coordination of the polymer sbl-2D-P6MOCN (2D-R_p and 2D-S_p). Noncoordinated solvent molecules were omitted.

The experimental powder X-ray diffraction (PXRD) patterns of **ml-2D-P5MOCN**, **bl-2D-P5MOCN**, **bl-2D-P6MOCN**, **sbl-2D-P6MOCN**, **fl-2D-P6MOCN** and **mtl-2D-P6MOCN** matched well with the simulated data satisfactorily, confirming their crystallinity (Fig. S19†). An interesting phenomenon is that the configurations of four 1,4-dimethoxybenzene units of **P5PhPy2** in **P5PhPy2Cu-3**, two 1,4-dimethoxybenzene units of **P5PhPy4** in **ml-2D-P5MOCN** and two 1,4-diethoxybenzene units of **P6PhPy4** in **fl-2D-P6MOCN** were reversed under the coordination at 80 °C. Pillararene host structures in **P5PhPy2Cu-3**, **ml-2D-P5MOCN** and **fl-2D-P6MOCN** were also relatively rare partially reversed crystal examples of pillararene derivatives at high temperatures.[36–38] ^{1}H NMR variable-temperature experiments were carried out to get insight into the transformation of **P5PhPy2** and **P5PhPy4** in DMSO-d6 and **P6PhPy4** in DMF-d7 by changing temperature (Fig. S20–S22†). 2D NOESY and COSY experiments were recorded for **P5PhPy2** and **P5PhPy4** in DMSO-d6 and **P6PhPy4** in DMF-d7 to assign the signals at room temperature (Fig. S23–S28†). The changes in the signals of 1,4-dimethoxybenzene or 1,4-diethoxybenzene units and methylene groups were very obvious, while the signal change of the phenylpyridine groups was relatively small, which may be rationalized by considering that 1,4-dimethoxybenzene and 1,4-diethoxybenzene units in part were rotated sharply and alternately, and the phenylpyridine units of **P5PhPy2**, **P5PhPy4** and **P6PhPy4** were shaking violently with increasing temperature. ^{1}H NMR variable-temperature experiments for **P5PhPy4** in $CDCl_3$ and **P6PhPy4** in $CDCl_3$ and DMSO-d6 (low solubility) were also performed (Fig. S29–S31†). The variable-temperature results showed that whether in $CDCl_3$, DMSO-d6 or DMF, **P5PhPy4** and **P6PhPy4** showed similar chemical shift changes. The adiponitrile@**P6PhPy4** in DMF-d7 was also tested at room temperature and 80 °C (Fig. S32†), and the experiment results showed that the introduction of guests can inhibit the rotation of 1,4-diethoxybenzene units. The variable-temperature experiments confirmed that the mechanism of this inversion was related to factors such as temperature and guest molecules. While with the introduction of coordination, guests and solvents, as the number of bulky conjugated moieties on pillararenes increases, these rotations may be limited, fewer repeat units turned over at high temperatures, and some did not even turn over, which was why the pillar[6]arene units of **bl-2D-P6MOCN**, **sbl-2D-P6MOCN** and **mtl-2D-P6MOCN** did not undergo partial switching at 80 °C.

The crystal structure of **bl-2D-P6MOCN** and **sbl-2D-P6MOCN** showed that a single chiral two-dimensional plane could be formed through a single chiral pillararene (R_p or S_p), and the symmetrical tetra-functionalized pillar[6]arene may also provide one platform for the construction of multiple 2D chiral bilayer polymers (2D-*R* and 2D-*S*). Due to the bulky conjugated moiety on **P6PhPy4**, the interconversion of enantiomers of **P6PhPy4** was inhibited and then the enantiomers ***R*-P6PhPy4** and ***S*-P6PhPy4** were obtained by chiral high-performance liquid chromatography. Two peaks with nearly equal areas were observed by chiral HPLC, and these two fractions were collected

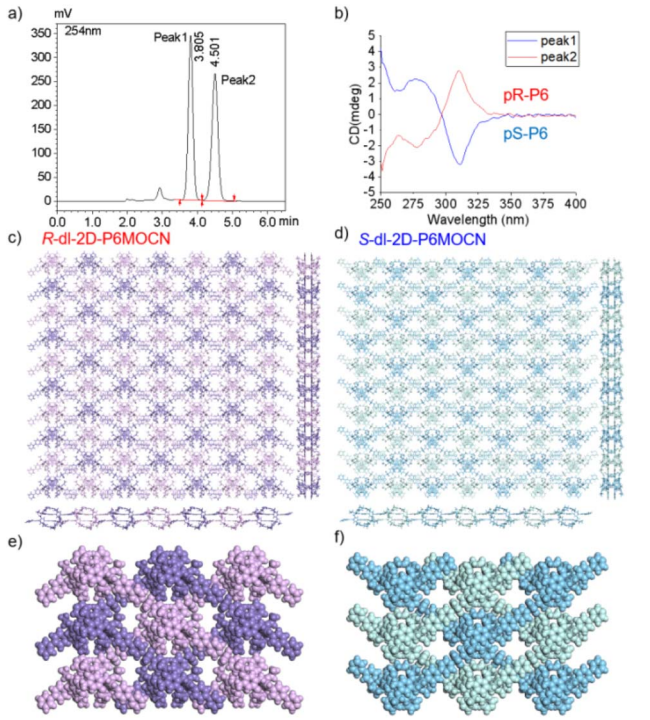

Fig. 8 (a) Resolution of the enantiomers of P6PhPy4 by chiral HPLC. (b) CD spectra of *S*-P6PhPy4 (blue line) and *R*-P6PhPy4 (red line) in dichloromethane. (c and d) The crystal structure bilayer 2D coordination of the polymers *R*-bl-2D-P6MOCN and *S*-bl-2D-P6MOCN. (e and f) The up and down entanglement pattern of *R*-bl-2D-P6MOCN and *S*-bl-2D-P6MOCN. Noncoordinated solvent molecules were omitted.

as optically pure P6 enantiomers (Fig. 8a and b and S33–S35†). The P6 enantiomers had a consistent NMR spectrum and similar UV and fluorescence spectra (Fig. S36 and S37†). We cultured ***R*-P6PhPy4** or ***S*-P6PhPy4** with Cu(II) nitrate in DMF under the same conditions as **bl-2D-P6MOCN**, and then we got two chiral two-dimensional bilayer structure products ***R*-bl-2D-P6MOCN** and ***S*-bl-2D-P6MOCN** (Fig. 8c and d), respectively. The arrangement patterns of ***R*-bl-2D-P6MOCN** and ***S*-bl-2D-P6MOCN** were similar to that of **bl-2D-P6MOCN**, and the torsional angle of the two straight ligands approached 120° with a form of parallel up and down crossing (Fig. 8c–f) and pillar[6]arene units showed a twisted hexagonal structure, while the coordination pattern of Cu(II) in ***R*-bl-2D-P6MOCN** or ***S*-bl-2D-P6MOCN** was similar to that of **sbl-2D-P6MOCN** and **mtl-2D-P6MOCN**, a –Cu–**P6PhPy4**–Cu–**P6PhPy4**– model, where the Cu(II) atom was six-coordinate, bonded by two pyridine N atoms from two different **P6PhPy4** ligands (Cu–N, 1.986–2.008 Å) and four oxygen donors from two COO^- ions (Cu–O, 2.006–2.565 Å). Two bilayer structures formed a denser bilayer braided two-dimensional structure by interpenetration, which means that the molecular woven network adopted the overlying weaving mode with the up-and-down entanglement mode, and the bilayer braided two-dimensional network was stacked in the form of AB stacking arrangement layer by layer (Fig. S38†). The π···π interaction between the benzene ring of pillar[6]enes in the upper layer and the pyridine ring of the ligand in the lower layer and the C–H···π interaction between methylene of pillar[6]enes in the upper layer and the benzene ring of the ligand in the lower layer were the main reasons to form the AB stacking arrangement (Fig. S38†). The experimental powder X-ray diffraction (PXRD) patterns of ***R*-bl-2D-P6MOCN** and ***S*-bl-2D-P6MOCN** not only had the same diffraction peaks but also matched with the simulated data satisfactorily, confirming their crystallinity (Fig. S39†). The CD spectra of ***R*-bl-2D-P6MOCN** (red line) and ***S*-bl-2D-P6MOCN** (blue line) in the solid state further confirmed the single chiral 2D structure (Fig. S40†). The assembly of two-dimensional chiral pillararene-type structures provided a new method for the construction of 2D mono-, bi-, and multi-layer chiral planar polymers and chiral molecular woven structures.

The morphologies of **ml-2D-P5MOCN**, **bl-2D-P5MOCN**, **bl-2D-P6MOCN**, **sbl-2D-P6MOCN**, **fl-2D-P6MOCN**, **mtl-2D-P6MOCN**, ***R*-bl-2D-P6MOCN** and ***S*-bl-2D-P6MOCN**, which were prepared by using the ultrasonic diffusion method, were further investigated by transmission electron microscopy (TEM) and by tapping-mode atomic force microscopy (AFM). Interestingly, the TEM images of these 2D **PMOCNs** showed clear sheet morphology structures in the form of multilayer stacking and the clear lattice fringes further indicated that these 2D PMOCNs had high crystallinity (Fig. 9a–h and S41–S48†). Aliquots (10 μL) of the micellar solution prepared by the ultrasonic diffusion method as described were deposited on a single-face-polished silicon wafer substrate and dried at room temperature *in vacuo* (Fig. 9i–p and S49–S56†). Height-vs-distance analysis indicated that the flakes of **ml-2D-P5MOCN**, **bl-2D-P5MOCN**, **bl-2D-P6MOCN**, **sbl-2D-P6MOCN**, **fl-2D-P6MOCN**, ***R*-bl-2D-P6MOCN** and ***S*-bl-2D-P6MOCN** exhibited a thickness of around 0.9 nm, 0.9 nm, 1.0 nm, 1.5 nm, 2.5 nm, 0.9 nm and 0.9 nm, respectively, which well matched with the calculated height (1.0 nm, 1.0 nm, 1.2 nm, 1.3 nm, 2.1 nm, 1.1 nm and 1.1 nm) of the set of **PMOCNs**. Due to the multilayer structure of **mtl-2D-P6MOCN**, the thickness (10.0–17.0 nm) was significantly higher than that of other networks. The thickness of these coordination polymeric arrays also validated that the structure of the networks constructed from macrocycles provided an excellent method to control the thickness of the flakes.

The networks of **ml-2D-P5MOCN**, **bl-2D-P5MOCN**, **bl-2D-P6MOCN**, **sbl-2D-P6MOCN**, **fl-2D-P6MOCN** and **mtl-2D-P6MOCN** changed easily with temperature in the thermal analysis experiment (Fig. S57†) and showed no adsorption effect of nitrogen at 77 K (Fig. S58†). The adsorption capacity of carbon dioxide of **ml-2D-P5MOCN**, **bl-2D-P5MOCN**, **bl-2D-P6MOCN**, **sbl-2D-P6MOCN**, **fl-2D-P6MOCN** and **mtl-2D-P6MOCN** was 14.46, 10.99, 24.66, 5.58, 9.56, and 6.38 $cm^3\ g^{-1}$ at 273 K, respectively (Fig. S59†). Because these networks were able to maintain order in H_2O, acetone and methanol for 12 h (Fig. S60†) and considering the solubility of **P5PhPy4** and **P6PhPy4** in methanol, we chose to directly carry out the adsorption experiment of the aqueous phase after obtaining crystals. The crystals of **ml-2D-P5MOCN**, **bl-2D-P5MOCN**, **bl-2D-P6MOCN**, **sbl-2D-P6MOCN**, **fl-2D-P6MOCN** and **mtl-2D-P6MOCN** were all subjected to iodine adsorption experiments

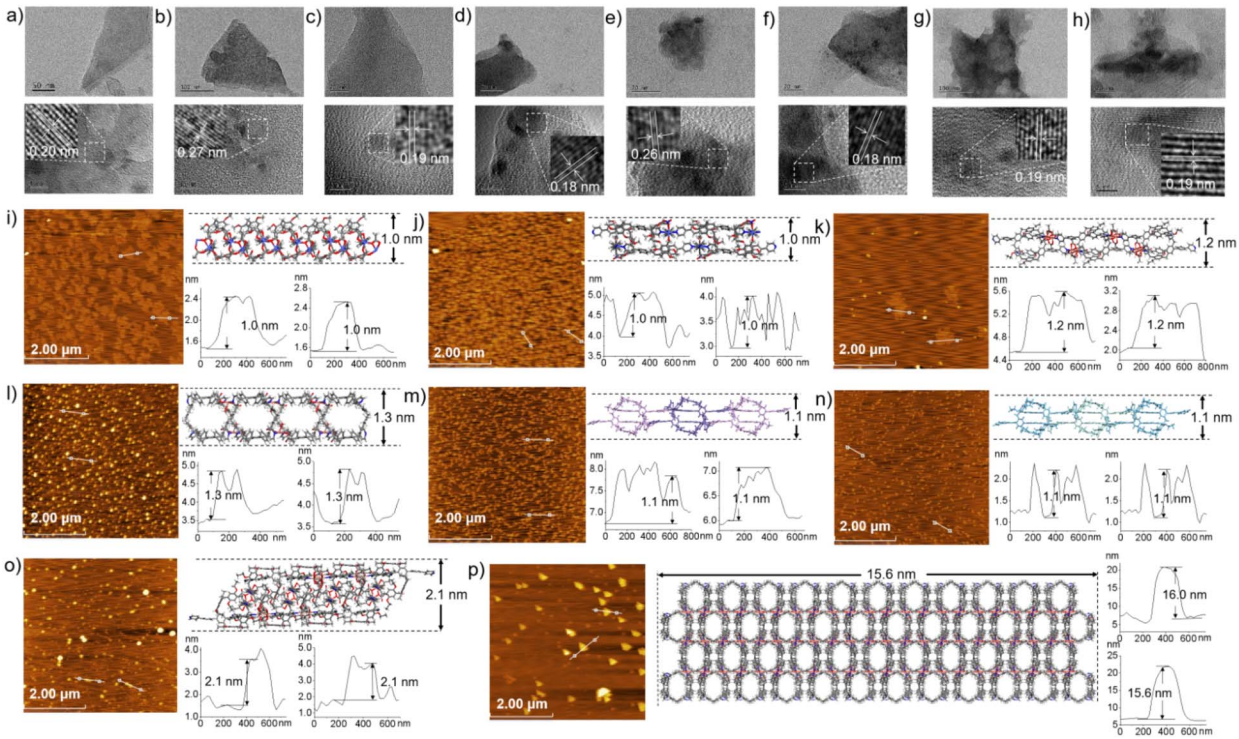

Fig. 9 TEM images of **ml-2D-P5MOCN**, **bl-2D-P5MOCN**, **bl-2D-P6MOCN**, **sbl-2D-P6MOCN**, **fl-2D-P6MOCN**, **mtl-2D-P6MOCN**, ***R*-bl-2D-P6MOCN** and ***S*-bl-2D-P6MOCN** (a–h). AFM images of **ml-2D-P5MOCN**, **bl-2D-P5MOCN**, **bl-2D-P6MOCN**, **sbl-2D-P6MOCN**, ***R*-bl-2D-P6MOCN**, ***S*-bl-2D-P6MOCN**, **fl-2D-P6MOCN**, and **mtl-2D-P6MOCN** flakes with a thickness of around 1.0 nm, 1.0 nm, 1.2 nm, 1.3 nm, 1.1 nm, 1.1 nm, 2.1 nm and 15.6 nm, respectively (i–p).

in water at room temperature (Fig. S61–S64†). A time-dependent UV/vis experiment showed that upon the addition of 1.0 mg of **ml-2D-P5MOCN**, **bl-2D-P5MOCN**, **bl-2D-P6MOCN**, **sbl-2D-P6MOCN**, **fl-2D-P6MOCN** and **mtl-2D-P6MOCN**, the aqueous solution of I_2 (1.0 mM, 2.5 mL) changed from yellowish brown to colourless transparent, and the crystals changed from pink and green or blue to reddish-brown, the adsorption rates of I_2 were 96.59%, 93.36%, 95.42%, 93.59%, 93.32% and 97.12%, respectively, and the final adsorption capacity was 1.83 mg mg^{-1}, 1.80 mg mg^{-1}, 1.73 mg mg^{-1}, 1.84 mg mg^{-1}, 1.53 mg mg^{-1} and 1.90 mg mg^{-1}, respectively, demonstrating their excellent iodine adsorption properties (Fig. 10a and S65†). More interesting, the PXRD profiles of $I_2 \subset$ **ml-2D-P5MOCN** and $I_2 \subset$ **bl-2D-P5MOCN** suggested that the two networks were transformed from a crystalline form to an amorphous form, with no diffraction peak observed at 3–50° (Fig. S66a and b†). These results indicated that the structures of **ml-2D-P5MOCN** and **bl-2D-P5MOCN** may have been interrupted upon I_2 adsorption, which may be attributed to the deformed cavity of pillar[5]arene and N···I, O···I and Co···I bonding interactions.[39,40] The diffraction peak of $I_2 \subset$ **P6MOCNs** can still be observed (Fig. S66c–f†), confirming that the crystalline form of these **P6MOCNs** was maintained with higher stability compared to **P5MOCNs**, which may be related to the cavity of **P6PhPy4**, since the twisted hexagonal structure and perfect well-maintained hexagonal structure were the structures in which they could exist stably. Fortunately, we obtained the crystal structure of **mtl-2D-P6MOCN** after iodine adsorption in water, and the cell parameters were consistent with **mtl-2D-P6MOCN** (Table S5†). Due to the solvent exchange of the crystal, the main structure of the network had not changed except that the anion coordinated with Cu(II) had become a water molecule (Fig. 10b), and the disordered iodine ions were distributed in the cavities and pores (Fig. 10c and d and S67†), which further confirmed the stability of **P6MOCNs** relative to **P5MOCNs** in water. The crystal structure showed that one reason for iodine adsorption may be the host–guest interaction of the cavity of pillararenes. To obtain more information on the interaction between the PMONs and iodine species, FT-IR spectra, X-ray photoelectron spectroscopy (XPS) and Raman spectroscopy were employed. The FT-IR spectra showed an obvious change in the area of the stretching vibration peaks of the C=O bonds of the coordinate carboxylate group and the peaks of the C=C/C–H bonds of the benzene rings in all the PMONs after iodine adsorption, indicating that there are strong interactions between the adsorbed iodine and the C=O bonds and aromatic rings within the PMONs (Fig. S68†). The XPS spectra of these PMONs after iodine adsorption showed characteristic peaks, further indicating the interactions between PMONs and the adsorbed iodine species (Fig. S69†).[41,42] Two prominent peaks located at 629.0 and 616.9 eV for **ml-2D-P5MOCN**, 625.9 and 613.9 eV for **bl-2D-P5MOCN**, 628.9 and 616.9 eV for **fl-2D-P6MOCN**, and 628.9 and 617.9 eV for **mtl-2D-P6MOCN**, one weak peak at 614.9 eV for **bl-2D-P6MOCN**, and two weak peaks located at

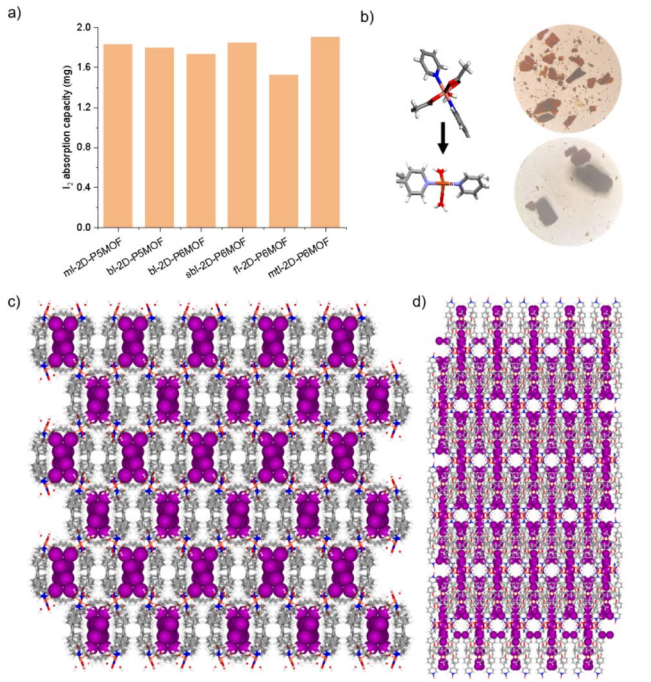

Fig. 10 (a) The final iodine adsorption capacity (1.0 mM, 10 mL) of **ml-2D-P5MOCN**, **bl-2D-P5MOCN**, **bl-2D-P6MOCN**, **sbl-2D-P6MOCN**, **fl-2D-P6MOCN** and **mtl-2D-P6MOCN** in aqueous solution (the amount of each network was 1 mg). (b–d) The crystal structure of **mtl-2D-P6MOCN** after iodine adsorption in water. Noncoordinated solvent molecules were omitted.

628.9 and 617.9 eV for **sbl-2D-P6MOCN** were observed, which can be assigned to the I $3d_{3/2}$ and I $3d_{5/2}$ orbitals of iodine molecules, indicating that the captured iodine species in the PMONs were mainly in their molecule form. Raman spectroscopic measurements were conducted to further detect the adsorbed iodine species. No visible peaks were observed in the Raman spectra of these networks before iodine adsorption. Two characteristic peaks at 110 and 168 cm^{-1} for **ml-2D-P5MOCN**, **bl-2D-P5MOCN**, **sbl-2D-P6MOCN**, **fl-2D-P6MOCN** and **mtl-2D-P6MOCN** and 108 and 170 cm^{-1} for **bl-2D-P6MOCN** were observed after iodine capture (Fig. S70†). These peaks were attributed to the symmetric and asymmetric stretching vibrations of polyiodine anions (I_3^- and I_5^-),[41,42] and the generation of iodine polyanions also indicated that charge transfer occurred, because of the strong interactions between the structures of PMONs and iodine. FT-IR, XPS, and Raman spectra demonstrated that there were strong interactions between PMONs and the adsorbed iodine species. More importantly, the set of **P6MOCNs** could adsorb iodine directly from the aqueous environment at ambient temperature and maintain the same structure, expanding the application and research of pillararene-type metal–organic coordination networks.

Conclusions

In summary, we have achieved 2D monolayer, bilayer, four-layer and multilayer coordination polymeric arrays *via* facile supramolecular self-assembly processes using two conjugated pillararenes **P5PhPy4** and **P6PhPy4**. Pillar[5]arene and pillar[6]arene units were used as excellent tunable scaffolds for structural regulation to precisely construct ladder-like monolayer, square-grid bilayer, sandwich bilayer, four-layer and multi-layer supramolecular networks. Single crystal structures confirmed changes in the configuration of pillararenes as the network changes. Single crystal structures also confirmed that the repeating units of pillar[5]arene and pillar[6]arene could be partially rotated in the networks under heating conditions and coordination. The enantiomers ***R*-P6PhPy4** and ***S*-P6PhPy4**, obtained by high-performance liquid chromatography, could also be used as excellent units to precisely construct a 2D bilayer chiral polymer array. Atomic force microscopy imaging confirmed the ultrathin thicknesses of these 2D materials. The structures of 2D P5MOCNs and P6MCONs exhibited excellent iodine adsorption properties in the aqueous phase at room temperature; especially pillar[6]arene-type networks were able to maintain the frame structure after iodine adsorption. From a crystal engineering and supramolecular chemistry perspective, this work not only provided a new strategy for developing more sophisticated and functional mono-, bi-, three-, four-, and multi-layer 2D materials and chiral two-dimensional materials but also provided reference models for the construction of complex bilayer networks with a specific thickness or number of layers, enriching the studies in supramolecular self-assembly of multiple types of multi-layer 2D nanomaterials. From a practical point of view, in addition to the adsorption function as adsorbents, we also hope that this field further develops towards the integration of pillararenes and functional ligands or modules into frameworks that can be responsive to pH, ions, light and electrons and then make progress in the fields of catalysis, energy conversion and biological functions.

Data availability

All characterization data and experimental protocols are provided in this article and the ESI Appendix. Crystallographic data have been deposited in the Cambridge Crystallographic Data Centre (CCDC) under accession numbers CCDC: 2244320 (for **P5PhPy4**), 2244321 (for **P5PhPy2**), 2244322 (for **P5PhPy2Cu-1**), 2244323 (for **P5PhPy2Cu-2**), 2244324 (for **P5PhPy2Cu-3**), 2244325 (for **P5PhPy2Cu-5**), 2244326 (for **P5PhPy2Co-1**), 2244327 (for **ml-2D-P5MOCN**), 2244328 (for **bl-2D-P5MOCN**), 2326170 (for **P6PhPy4**), 2326171 (for **bl-2D-P6MOCN**), 2342430 (for **sbl-2D-P6MOCN**), 2326172 (for **sbl-2D-P6MOCN**), 2326174 (for **fl-2D-P6MOCN**), 2326175 (for **mtl-2D-P6MOCN**), 2326165 (for I_2@**mtl-2D-P6MOCN**), 2326166 (for ***R*-bl-2D-P6MOCN**), and 2326167 (for ***S*-bl-2D-P6MOCN**). These data can be obtained free of charge from the Cambridge Crystallographic Date Centre *via* https://www.ccdc.cam.ac.uk/datarequest/cif.† Extra data are available from the corresponding author upon request.

Author contributions

B. Y. and Z. T. L. conceptualized the ideas and supervised the investigations; Z. N. C. and L. P. Z. performed the synthesis and

X-ray single crystal diffraction, TEM, AFM, PXRD and iodine adsorption experiments; H. L. W. and M. Y. performed ^{1}H NMR variable-temperature, 2D NOESY and COSY experiments. Z. N. C., L. P. Z., and B. Y. collected the data; Q. Y. Q. and B. Y. drew the schematic diagram; Z. N. C., L. P. Z., B. Y., J. T., G. Y. Y. and Z. T. L. analysed the data; B. Y. and Z. T. L. finished the writing.

Conflicts of interest

There are no conflicts to declare.

Acknowledgements

We thank the National Natural Science Foundation of China (No. 22201268) for financial support.

Notes and references

1 K. S. Novoselov, A. K. Geim, S. V. Morozov, D. Jiang, Y. Zhang, S. V. Dubonos, I. V. Grigorieva and A. A. Firsov, *Science*, 2004, **306**, 666–669.
2 M. Xu, T. Liang, M. Shi and H. Chen, *Chem. Rev.*, 2013, **113**, 3766–3798.
3 C. Tan, X. Cao, X.-J. Wu, Q. He, J. Yang, X. Zhang, J. Chen, W. Zhao, S. Han, G.-H. Nam, M. Sindoro and H. Zhang, *Chem. Rev.*, 2017, **117**, 6225–6331.
4 P. You, G. Tang and F. Yan, *Mater. Today Energy*, 2019, **11**, 128–158.
5 J. Liang, H. Yu, J. Shi, B. Li, L. Wu and M. Wang, *Adv. Mater.*, 2023, **35**, 2209814.
6 G. Yu, K. Jie and F. Huang, *Chem. Rev.*, 2015, **115**, 7240–7303.
7 Y. Zhou, K. Jie, R. Zhao and F. Huang, *Adv. Mater.*, 2020, **32**, 1904824.
8 D. Xia, P. Wang, X. Ji, N. M. Khashab, J. L. Sessler and F. Huang, *Chem. Rev.*, 2020, **120**, 6070–6123.
9 X.-Q. Wang, W.-J. Li, W. Wang and H.-B. Yang, *Acc. Chem. Res.*, 2021, **54**, 4091–4106.
10 X. Li, H.-S. Xu, K. Leng, S. W. Chee, X. Zhao, N. Jain, H. Xu, J. Qiao, Q. Gao, I.-H. Park, S. Y. Quek, U. Mirsaidov and K. P. Loh, *Nat. Chem.*, 2020, **12**, 1115–1122.
11 Z.-J. Yin, S.-Y. Jiang, N. Liu, Q.-Y. Qi, Z.-Q. Wu, T.-G. Zhan and X. Zhao, *CCS Chem.*, 2022, **4**, 141–150.
12 B. Yang, S. B. Yu, P. Q. Zhang, Z. K. Wang, Q. Y. Qi, X. Q. Wang, X. H. Xu, H. B. Yang, Z. Q. Wu, Y. Liu, D. Ma and Z.-T. Li, *Angew. Chem., Int. Ed.*, 2021, **60**, 26268–26275.
13 T. Ogoshi, S. Kanai, S. Fujinami, T.-A. Yamagishi and Y. Nakamoto, *J. Am. Chem. Soc.*, 2008, **130**, 5022–5023.
14 T. Ogoshi, T. Kakuta and T.-A. Yamagishi, *Angew. Chem., Int. Ed.*, 2018, **58**, 2197–2206.
15 H. Zhang, Z. Liu and Y. Zhao, *Chem. Soc. Rev.*, 2018, **47**, 5491–5528.
16 N. Song, T. Kakuta, T.-A. Yamagishi, Y.-W. Yang and T. Ogoshi, *Chem*, 2018, **4**, 2029–2053.
17 T. Ogoshi, T.-A. Yamagishi and Y. Nakamoto, *Chem. Rev.*, 2016, **116**, 7937–8002.
18 L. Liu, Y. Hu, S. Huang, Y. Jin, J. Cui, W. Gong and W. Zhang, *Chem. Sci.*, 2021, **12**, 13316–13320.
19 W.-J. Li, W.-T. Xu, X.-Q. Wang, Y. Jiang, Y. Zhu, D.-Y. Zhang, X.-Q. Xu, L.-R. Hu, W. Wang and H.-B. Yang, *J. Am. Chem. Soc.*, 2023, **145**, 14498–14509.
20 M.-H. Li, C.-L. Xu and Y.-W. Yang, *Coord. Chem. Rev.*, 2024, **512**, 215894.
21 X. Li, M.-L. Shen, J. Yang, L.-L. Liu and Y.-W. Yang, *Adv. Mater.*, 2024, **36**, 2313317.
22 Z.-Q. Wang, X. Wang and Y.-W. Yang, *Adv. Mater.*, 2024, **36**, 2301721.
23 X.-Y. Lou, S.-Y. Zhang, Y. Wang and Y.-W. Yang, *Chem. Soc. Rev.*, 2023, **52**, 6644.
24 N. L. Strutt, D. Fairen-Jimenez, J. Iehl, M. B. Lalonde, R. Q. Snurr, O. K. Farha, J. T. Hupp and J. F. Stoddart, *J. Am. Chem. Soc.*, 2012, **134**, 17436–17439.
25 N. L. Strutt, H.-C. Zhang and J. F. Stoddart, *Chem. Commun.*, 2014, **50**, 7455–7458.
26 E. Lee, I. H. Park, H. Ju, S. Kim, J. H. Jung, Y. Habata and S. S. Lee, *Angew. Chem., Int. Ed.*, 2019, **58**, 11296–11300.
27 H. Zhu, Q. Li, B. Shi, H. Xing, Y. Sun, S. Lu, L. Shangguan, X. Li, F. Huang and P. J. Stang, *J. Am. Chem. Soc.*, 2020, **142**, 17340–17345.
28 X.-Y. Lou and Y.-W. Yang, *J. Am. Chem. Soc.*, 2021, **143**, 11976–11981.
29 Y. Wu, M. Tang, Z. Wang, L. Shi, Z. Xiong, Z. Chen, J. L. Sessler and F. Huang, *Nat. Commun.*, 2023, **14**, 4927.
30 X. Wan, S. Li, Y. Tian, J. Xu, L.-C. Shen, H. Zuilhof, M. Zhang and A. C. H. Sue, *Chem*, 2022, **8**, 2136–2147.
31 M. Pan and M. Xue, *Eur. J. Org. Chem.*, 2013, 4787–4793.
32 H. Zeng, P. Liu, H. Xing and F. Huang, *Angew. Chem., Int. Ed.*, 2022, **61**, e202115823.
33 B. Yang, J.-W. Zhang, S.-B. Yu, Z.-K. Wang, P.-Q. Zhang, X.-D. Yang, Q.-Y. Qi, G.-Y. Yang, D. Ma and Z.-T. Li, *Sci. China: Chem.*, 2021, **64**, 1228–1234.
34 Q.-Y. Huang, W.-L. Li, Z. Mao, H. Zhang, Y. Li, D.-Y. Ma, H.-Y. Wu, J. Zhao, Z.-Y. Yang, Y. Zhang, L. Gong, M. P. Aldred and Z.-G. Chi, *Chem*, 2021, **5**, 1321–1332.
35 M. Li, B. Hua, H. Liang, J. Liu, L. Shao and F. Huang, *J. Am. Chem. Soc.*, 2020, **142**, 20892–20901.
36 J.-B. Yao, W.-H. Wu, W.-T. Liang, Y.-J. Feng, D.-Y. Zhou, J. J. Chruma, G. Fukuhara, T. Mori, Y. Inoue and C. Yang, *Angew. Chem., Int. Ed.*, 2017, **56**, 6869–6873.
37 S. Fa, K. Egami, K. Adachi, K. Kato and T. Ogoshi, *Angew. Chem., Int. Ed.*, 2020, **59**, 20353–20356.
38 J. Yao, W.-H. Wu, C. Xiao, D. Su, Z.-H. Zhong, T. Mori and C. Yang, *Nat. Commun.*, 2021, **12**, 2600.
39 G. Cavallo, P. Metrangolo, R. Milani, T. Pilati, A. Priimagi, G. Resnati and G. Terraneo, *Chem. Rev.*, 2016, **116**, 2478–2601.
40 Y. Lin, X. Jiang, S. T. Kim, S. B. Alahakoon, X. Hou, Z. Zhang, C. M. Thompson, R. A. Smaldone and C. Ke, *J. Am. Chem. Soc.*, 2017, **139**, 7172–7175.
41 K. Cheng, H.-L. Li, Z.-Y. Li, P.-Z. Li and Y. L. Zhao, *ACS Mater. Lett.*, 2023, **5**, 1546–1555.
42 X.-F. Li, Z.-M. Jia, J. Zhang, Y.-D. Zou, B. Jiang, Y.-D. Zhang, K.-W. Shu, N. Liu, Y. Li and L.-J. Ma, *Chem. Mater.*, 2022, **34**, 11062–11071.